PERGAMON

International Journal of Solids and Structures 38 (2001) 8653–8671

INTERNATIONAL JOURNAL OF SOLIDS and STRUCTURES

www.elsevier.com/locate/ijsolstr

Modeling of the thermomechanical behavior of porous shape memory alloys

Muhammad A. Qidwai [a], Pavlin B. Entchev [b], Dimitris C. Lagoudas [b,*], Virginia G. DeGiorgi [c]

[a] *Geo-Centers, Inc., Washington Operations, Multifunctional Materials Branch, Naval Research Laboratory, 4555 Overlook Avenue SW, Washington, DC 20375, USA*

[b] *Center for Mechanics of Composites, Department of Aerospace Engineering, Texas A&M University, College Station, TX 77843-3141, USA*

[c] *Multifunctional Materials Branch, Naval Research Laboratory, 4555 Overlook Avenue SW, Washington, DC 20375, USA*

Received 10 December 2000; in revised form 1 May 2001

Abstract

Two methods are used in this work to estimate the porous shape memory alloy (SMA) thermomechanical behavior. The porous SMA is assumed to be made of two components, the dense SMA matrix and the pores. An existing rate-independent type constitutive model is employed to describe the matrix behavior. Two contrasting strategies are used to estimate the overall thermomechanical behavior: (1) the unit cell finite element method (UCFEM) to account for periodic distribution of pores in the SMA matrix, and (2) an averaging micromechanics method based on the incremental formulation of the Mori–Tanaka method to account for random distribution of pores in the matrix. Cylindrical and spherical shapes are considered as approximations of open and closed pores, respectively, in both methods. Results are presented for both types of pores and comparisons are made between the two methods under various loading conditions. Both methods compare well in predicting the isothermal elastic material properties and pseudoelastic response under axial and out-of-plane shear loading. However, the transformation results differ under transverse and in-plane shear loading. This difference is found to be due to the use of an average value of stress for the SMA matrix in the micromechanics averaging method, which diminishes the effect of local stress concentration thereby delaying the onset of phase transformation caused by an applied load. On the other hand, the actual values of stress at all material points in the SMA matrix are used in the UCFEM causing phase transformation in regions near the pores at smaller applied load values than what is calculated by the micromechanics averaging method. © 2001 Published by Elsevier Science Ltd.

Keywords: Porous shape memory alloy; Smart material; Micromechanics averaging method; Periodic unit cell; Constitutive behavior; Pseudoelasticity

* Corresponding author. Tel.: +1-979-845-7541; fax: +1-979-845-6051.

E-mail addresses: qidwai@anvil.nrl.navy.mil (M.A. Qidwai), pavlin@aero.tamu.edu (P.B. Entchev), lagoudas@aero.tamu.edu (D.C. Lagoudas), degiorgi@anvil.nrl.navy.mil (V.G. DeGiorgi).

0020-7683/01/$ - see front matter
PII: S0020-7683(01)00118-4

1. Introduction

Dense shape memory alloys (SMAs) have been used as active materials in smart structures for more than a decade now, and they have captured the imagination of the engineering community since the early sixties (Buehler et al., 1963; Buehler and Wiley, 1965; Wayman, 1983). During the last 15 years a number of research papers on constitutive modeling of dense SMAs has appeared in the literature. Some representative works have been published by Tanaka (1986), Liang and Rogers (1990, 1992), Brinson and Lammering (1993), Graesser and Cozzarelli (1994), Boyd and Lagoudas (1996), Lagoudas et al. (1996), Levitas (1998), Govindjee and Hall (1999) and Qidwai and Lagoudas (2000b). Additional papers can be found in the review paper by Birman (1997).

Initiating from early studies in Russia (Shabalovskaya et al., 1994; Itin et al., 1994; Shevchenko et al., 1997) and further development in China (Li et al., 1998a,b, 1999), porous SMAs have been developed and used primary for bone reconstruction applications (Simske et al., 1996; Ayers et al., 1999). They have lower density compared to fully dense SMAs, which allows their use in a number of lightweight applications. Another advantage of porous SMAs is the possibility of creating a functionally gradient material by spatially varying the porosity. The expectation is that the porous SMAs will retain some of the desirable characteristics of fully dense SMAs, e.g., shape memory effect and pseudoelasticity while enhancing shape recovery and energy absorption capabilities.

In order to capitalize on the potential and unique capabilities offered by porous SMAs, it is necessary to establish efficient and accurate theoretical models and to develop experimental procedures for fabrication and testing of porous SMA specimens under quasi-static and dynamic loading. While both theoretical and experimental work are equally important, the current study focuses on the micromechanical modeling of porous SMAs under quasi-static loading, while detailed description of the material fabrication process can be found in other references (in addition to the above references, see, for example, Lagoudas et al., 2000b; Vandygriff et al., 2000; Thangaraj et al., 2000).

In order to effectively use the porous materials in various engineering areas, it is pertinent to know their mechanical and physical properties as a function of the pore volume fraction as well as the pore geometry and, possibly, pore distribution. Moreover, having effective methods for analyzing porous materials assists in designing new materials with specific properties. There is a great number of research papers available in the literature devoted to modeling of porous materials. Different aspects of modeling of porous and cellular solids are presented by Green (1972), Gurson (1977), Jeong and Pan (1995), Gibson and Ashby (1997), among others.

As seen from the literature review, the modeling of porous materials has been performed assuming either periodic or random distribution of pores. Even though the existence of periodic arrangement of pores in a real porous SMA material is an approximation, this assumption provides insight into global material behavior in the form of useful limiting values for the overall properties. Additionally, an approximate local variation of various field variables like stress and strain indicating areas of concentration due to porosity can be obtained. These results may provide design limitations in order to minimize or even avoid microbuckling, plastic yielding and consequently loss of phase transformation capacity over number of loading cycles. The assumption of periodicity and symmetry boundary conditions reduce the analysis of the porous SMA material to the analysis of a unit cell (Achenbach and Zhu, 1990; Nemat-Nasser and Hori, 1993; Lagoudas et al., 1996). Thus, appropriate loading conditions need to be applied, which do not violate the symmetry of the problem.

Micromechanical averaging techniques can also be used to determine the averaged macroscopic response of the porous material with random distribution of pores. In this case the material is treated as a composite with two phases: dense matrix and pores. Among the micromechanics averaging methods, the two most widely used are the self-consistent method and the Mori–Tanaka method (MTM). Both approaches are based on the presumption that the effective response of the composite can be obtained by considering a single inhomogeneity embedded in an infinite matrix.

According to the self-consistent method (Hershey, 1954; Kröner, 1958; Budiansky, 1965; Hill, 1965) the interactions between the inhomogeneities are taken into account by associating the properties of the matrix with the effective properties of the composite, i.e., embedding the inhomogeneity in an effective medium. Some self-consistent results for spherical pores in an incompressible material are presented by Budiansky (1965). Contrary to this approach, the MTM initially suggested by Mori and Tanaka (1973) and further developed by Weng (1984) and Benveniste (1987) takes into account the interactions between the inhomogeneities by appropriately modifying the average stress in the matrix from the applied stress, while the properties of the matrix are associated with the real matrix phase.

Recently, both averaging approaches have been applied to obtain effective properties of composites with inelastic phases. For example, a variant of the self-consistent method using incremental formulation (Hutchinson, 1970) has been used to model composites undergoing elastoplastic deformations. Lagoudas et al. (1991) have used an incremental formulation of the MTM to obtain the effective properties of a composite with an elastoplastic matrix and elastic fibers. In a different work, Lagoudas et al. (1994) have applied the incremental MTM to model the behavior of a composite with elastic matrix and SMA fibers. Another group of researchers (Cherkaoui et al., 2000) has applied the self-consistent technique to obtain the effective properties of a composite with elastoplastic matrix and SMA fibers.

Preliminary results of modeling of porous SMA based on both periodic pore distribution (using unit cell FEM) and random pore distribution (using micromechanics averaging technique) have been presented by the authors in conference proceedings (see Lagoudas et al., 2000a,b). Both modeling approaches are further developed and completed in this work. The purpose of the current effort is to present a comprehensive description of the two modeling methods. In addition, a thorough discussion and analysis of the obtained results will be performed.

The paper is organized as follows: Section 2.1 contains the description of the evaluation of quasi-static behavior of porous SMAs with the help of the unit cell finite element method (UCFEM) for periodically arranged open and closed pores in dense SMA matrix. Similarly, Section 2.2 describes the micromechanics averaging approach, based on the MTM for randomly arranged open and closed pores. Section 3 contains the numerical results for various pore volume fractions of both types of pores as calculated by the two methods. Both effective elastic material properties and transformation behavior are illustrated. Section 4 is devoted on discussion of the results. Finally, conclusions are presented in Section 5. The constitutive model for dense NiTi SMA is briefly described in the appendix.

2. Theoretical aspects of modeling

Porous SMA may contain all open pores, all closed pores or a combination of both types. In this study, either open or closed pores are assumed to exist in a given specimen. A micromechanical approach is used to determine the averaged macroscopic response regardless of pore type. The material is treated as a two-phase composite made of the dense SMA matrix and pores. The porous material is characterized by the pore volume fraction and the pore shape. The pore size is considered to be sufficiently larger than the lattice parameters of the SMA. It has been observed experimentally that the pore size is of the same order of magnitude as the grain size of Ni and Ti powders used for the fabrication of the porous SMA. Typical pore sizes are 100–1000 μm (Lagoudas et al., 2000b). The actual pore size does not enter neither in the UCFEM nor in the micromechanical averaging method. It should be noted that this is true for quasi-static loading, while the pore size will influence the dynamic response of the material.

The modeling of dense SMA matrix is carried out using an existing rate-independent constitutive model (Lagoudas et al., 1996; Qidwai and Lagoudas, 2000a). The SMA constitutive model for isothermal conditions is briefly summarized in the Appendix A, while its details may be found in the cited references.

As a result of the modeling, the effective thermomechanical response of the porous SMA including pseudoelasticity and shape memory effect will be obtained in the form of

$$\dot{\Sigma}_{ij} = L_{ijkl}\dot{E}_{ijkl}. \tag{1}$$

In Eq. (1) above $\dot{\Sigma}_{ij}$ and $\dot{E}_{ij}$ are the effective stress and strain increments, respectively and L_{ijkl} is the effective tangent stiffness tensor. The components of L_{ijkl} will be obtained for different loading paths.

2.1. Unit cell finite element method

As a first step, an in-plane hexagonal arrangement of pores is assumed in the present study. The cross-section of such an arrangement for open pores is shown in Fig. 1. The x–y plane forms the cross-section of the material specimen and z is the out-of-plane axis running along the length of the specimen. As shown in the figure, the open pores are assumed to be in the form of cylinders with circular cross-section and generators parallel to the out-of-plane z-axis. The resultant material possesses transverse isotropy similar to that obtained for a random arrangement of similar cylinders. On the other hand, closed pores are assumed to be spherical in shape. It is further assumed that layers of hexagonal arrangement of spheres lie equally distant in the out-of-plane z-direction at distance l. The resultant material symmetry is decided by the ratio of d with other characteristic lengths.

Assuming that the applied loads do not violate the geometric symmetry of the unit cell, one of the many possible representative unit cells, which can be used to predict the overall effective behavior, is given in Fig. 2 for both open and closed pores, respectively. The cross-section of each unit cell is a rectangle with cross-section $w \times 2h$, where $h = 0.866w$, and length l. For both open and closed pore unit cells, l is assumed to be equal to w. For these dimensions, the overall material behavior will be transversely isotropic for both open and closed pores. The material symmetry of closed pore material is dependent on geometric characteristics. For instance, if layers of closed pores (spheres) are assumed to be lying equidistant at $l = 4h$ instead of $l = w$ then the overall material behavior would be isotropic.

The 3-fold geometric (reflection) symmetry of the porous material, which needs to be applied on both open and closed pore unit cells, can be explained based on the open pore unit cell schematic given by the

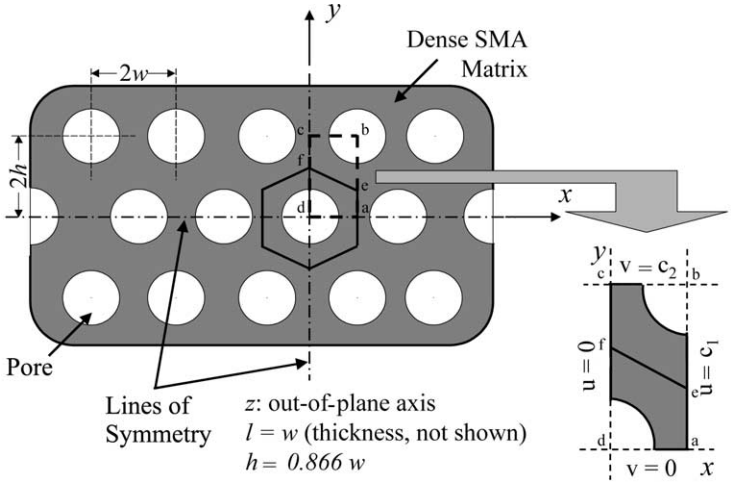

Fig. 1. Cross-sectional schematic of periodic hexagonal arrangement of open pores (cylinders) in a dense SMA matrix. The blown-out image is the cross-section view of the unit cell used in the analysis.

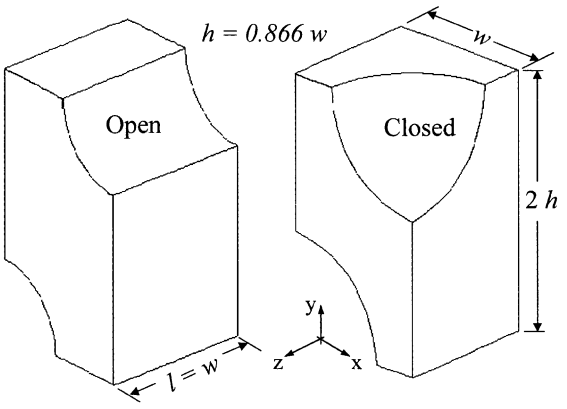

Fig. 2. 3-D open and closed pore unit cells used in the study. These unit cells completely define the behavior of their bulk counterparts.

dashed lines (a–b–c–d–a) in Fig. 1. Note that the unit cell has a uniform depth in the z-direction. The following displacement boundary conditions need to be applied regardless of pore geometry:

$$u(0,y,z) = v(x,0,z) = w(x,y,0) = 0, \tag{2}$$

$$u(w,y,z) = c_1, \quad v(x,2h,z) = c_2, \quad w(x,y,l) = c_3, \tag{3}$$

where (u, v, w) are displacements in the (x, y, z) directions, respectively, and c_1, c_2 and c_3 are constants, which impose the boundary conditions that all material points on respective unit cell boundaries have the same normal displacement. Similarly, the reflective symmetries imply that shear stress components vanish on all boundaries of the unit cell:

$$\sigma_{xy}(0,y,z) = \sigma_{xy}(w,y,z) = \sigma_{xy}(x,0,z) = \sigma_{xy}(x,2h,z) = 0, \tag{4}$$

$$\sigma_{xz}(x,y,0) = \sigma_{xz}(x,y,l) = \sigma_{xz}(0,y,z) = \sigma_{xz}(w,y,z) = 0, \tag{5}$$

$$\sigma_{yz}(x,y,0) = \sigma_{yz}(x,y,l) = \sigma_{yz}(x,0,z) = \sigma_{yz}(x,2h,z) = 0. \tag{6}$$

The stress and strain fields in the unit cell can be extended for the whole porous SMA material by virtue of the periodicity and symmetry conditions. The effective applied stress is obtained as the ratio of the total applied force to the area of the boundary of the unit cell. The effective strain is calculated as ratio of the displacement on the boundary of the unit cell to the initial length of the unit cell in the loading direction for different loading paths.

As mentioned in the beginning of Section 2, the modeling of the response of porous SMAs is independent on the pore size. Indeed, additional finite element computations were performed for self-similar pore shapes of different sizes, which reconfirmed the independence on pore size. The independence of the results on pore size can also be shown by normalizing the governing equations by the characteristic length of the unit cell (in this case, by the value of w).

2.2. Micromechanics averaging method

In this case the overall stress Σ_{ij} and strain E_{ij}, which are uniform over the representative volume element (RVE) are computed by volume averaging the corresponding local quantities (stress σ^m_{ij} and strain ε^m_{ij}). Thus, for a loading path given by $E_{ij}(t)$ the corresponding overall stress Σ_{ij} will be evaluated using a micromechanics averaging method. In this work, isothermal conditions are assumed and the description is

restricted to a two-phase composite, i.e., the SMA matrix and pores of identical shape. Thus the porous SMA is completely characterized by the volume fraction of the pores c_p and the pore shape. Following the standard micromechanics approach (Hill, 1965), the following relation exists between the globally applied increment of strain $\dot{E}_{ij}$ and the local increment of strain in the matrix $\dot{\varepsilon}^m_{ij}(x_n)$:

$$\dot{\varepsilon}^m_{ij}(x_n) = A^m_{ijkl}(x_n)\dot{E}_{kl}, \tag{7}$$

where $A^m_{ijkl}(x_n)$ is the matrix strain concentration factor and x_n are the components of the position vector. Taking the volume average of Eq. (7) results in

$$\dot{\varepsilon}^m_{ij} = \langle \dot{\varepsilon}^m_{ij}(x_n)\rangle = \langle A^m_{ijkl}(x_n)\rangle \dot{E}_{kl}. \tag{8}$$

The average matrix strain concentration factor $A^m_{ijkl} = \langle A^m_{ijkl}(x_n)\rangle$ is calculated from the following relation:

$$c_p A^p_{ijkl} + (1 - c_p)A^m_{ijkl} = \delta_{ijkl}, \tag{9}$$

where A^p_{ijkl} is the average strain concentration for the inhomogeneities (pores) and δ_{ijkl} is the fourth-order symmetric identity tensor, given by

$$\delta_{ijkl} = \tfrac{1}{2}(\delta_{ik}\delta_{jl} + \delta_{il}\delta_{jk}). \tag{10}$$

The pore strain concentration factor A^p_{ijkl} is evaluated using the Mori–Tanaka approximation (Weng, 1984; Benveniste, 1987; Lagoudas et al., 1991):

$$A^p_{ijkl} = [\delta_{ijkl} - (1 - c_p)S^E_{ijkl}]^{-1}, \tag{11}$$

where S^E_{ijkl} is the Eshelby tensor, defined for the shape of the pores and the dense SMA tangent stiffness tensor, L^m_{ijkl}. Therefore, the MTM, which has been developed for elastic heterogeneous media is implemented here in an incremental way.

After the local strain increment is evaluated from Eq. (8), the increment in local stress and volume fraction of martensite (ξ) are calculated by integrating the constitutive SMA response (Appendix A) using a return mapping algorithm (Qidwai and Lagoudas, 2000a). The numerical algorithm that incorporates the MTM and the return mapping algorithm is shown in Table 1.

Once the stress tensor, the transformation strain tensor, the martensitic volume fraction, the tangent stiffness and the average strain concentration factor in the SMA matrix are updated, the macroscopic (effective) tangent stiffness tensor L_{ijkl} as defined by Eq. (1) is obtained. Employing the relation

$$\dot{\sigma}^m_{ij} = L^m_{ijkl}\dot{\varepsilon}^m_{kl} = L^m_{ijkl}A^m_{klmn}\dot{E}_{mn} \tag{12}$$

Table 1
Implementation of the incremental MTM and return mapping algorithm for porous SMAs

1.	Calculate Eshelby tensor S^E_{ijkl} using the elastic stiffness matrix for SMA and pore geometry
2.	Calculate $A^{m(k)}_{ijkl}$ (k is the iteration counter) using: $A^{p(k)}_{ijkl} = [\delta_{ijkl} - (1 - c_p)S^E_{ijkl}]^{-1}$; $c_p A^{p(k)}_{ijkl} + (1 - c_p)A^{m(k)}_{ijkl} = \delta_{ijkl}$
3.	Using the given increment of the macroscopic strain tensor $\dot{E}_{ij}$ obtain the increment of the microscopic strain tensor in the matrix $\dot{\varepsilon}^{m(k)}_{ij} = A^{m(k)}_{ijkl}\dot{E}_{kl}$
4.	Perform return mapping algorithm to obtain $\dot{\sigma}^{m(k)}_{ij}$, $\dot{\varepsilon}^{tm(k)}_{ij}$ and $\dot{\xi}^{(k)}$
5.	Update $L^{m(k)}_{ijkl}$
6.	Calculate S^E_{ijkl} using $L^{m(k)}_{ijkl}$
7.	Calculate $A^{m(k+1)}_{ijkl}$ using the new value of S^E_{ijkl}
8.	If $\|A^{m(k+1)}_{ijkl} - A^{m(k)}_{ijkl}\| \leqslant TOL$ then go to step (9); else go to step (3)
9.	Assign $L^m_{ijkl} = L^{m(k)}_{ijkl}$, $A^m_{ijkl} = A^{m(k)}_{ijkl}$
10.	Exit

and using the definition of the macroscopic stress increment

$$\dot{\Sigma}_{ij} = \frac{1}{V}\int_V \dot{\sigma}_{ij}\,\mathrm{d}V = \frac{1}{V}\int_{V^m} \dot{\sigma}^m_{ij}\,\mathrm{d}V = (1-c_\mathrm{p})\dot{\sigma}^m_{ij}, \tag{13}$$

the macroscopic (effective) tangent stiffness is given by the following equation:

$$L_{ijkl} = (1-c_\mathrm{p})L^m_{ijmn}A^m_{mnkl} \tag{14}$$

in terms of the dense SMA tangent stiffness tensor and the average strain concentration factor of the SMA.

3. Numerical results

The numerical return-mapping algorithm developed by Qidwai and Lagoudas (2000a) is used to describe the dense SMA matrix constitutive behavior in the UCFEM. The algorithm is implemented in a user supplied material subroutine (UMAT) which is compiled with the commercial FEM package ABAQUS (1997). To obtain the effective response of the material, finite element analysis is performed on the unit cells (shown in Fig. 2) under various loading conditions. An example of the finite element meshes that are used in the study is given in Fig. 3 for pore volume fraction of 0.4 for periodic open and closed pore SMA.

Similarly, the algorithm based on the incremental MTM (see Table 1) is also developed in a modified UMAT. The Eshelby tensor, required to compute the concentration factors, is not available in closed form for the case of general loading because phase transformation introduces anisotropy of the tangent stiffness tensors. Therefore, a numerical evaluation of the Eshelby tensor is employed in this work. The algorithm for the numerical evaluation used here is the one developed by Gavazzi and Lagoudas (1990). The shape of the inclusions (pores) is specified by the three principal axes of the ellipsoid, a_1, a_2 and a_3. For the case of closed pores (spherical inclusions), the principal axes were set equal: $a_1 = a_2 = a_3$. For the case of open pores

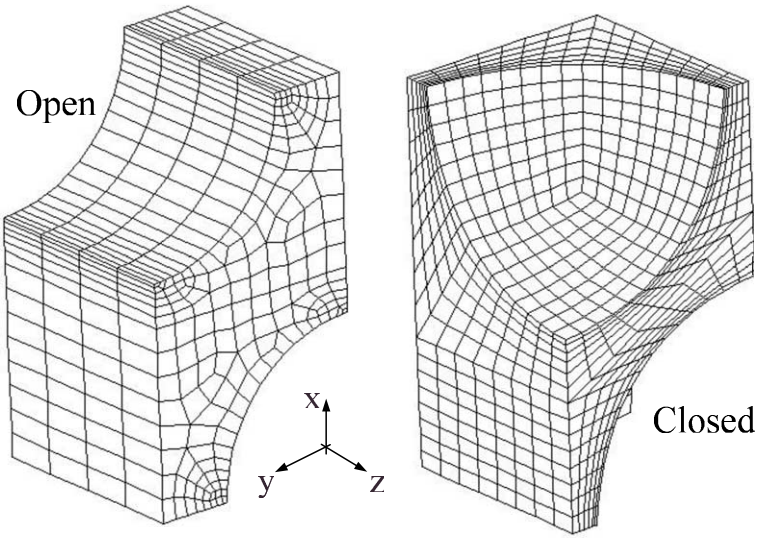

Fig. 3. Finite element meshes employed in the analyzes of periodic open and closed pore SMA, respectively, containing pore volume fraction of 0.4.

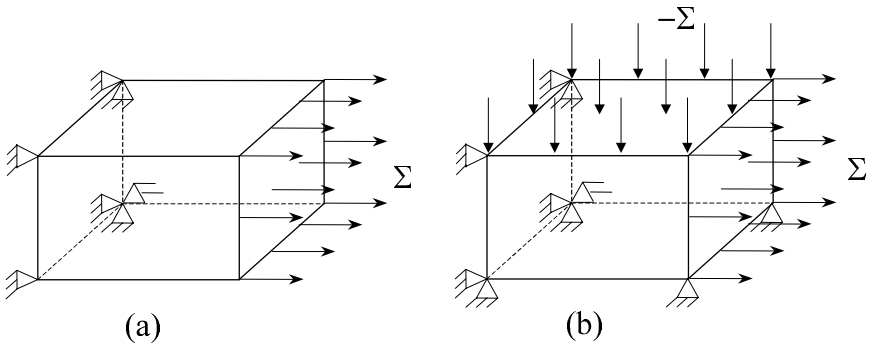

Fig. 4. Schematic of the boundary value problems used in the finite element implementation of the micromechanics averaging method: (a) tensile loading and (b) shear loading.

(cylindrical inclusions), two axes were set equal ($a_1 = a_2$) while the ratio a_3/a_1 was set equal to a very large number.

The effective constitutive response of porous SMA is obtained for axial, transverse, in-plane shear and out-of-plane shear loading cases for both the UCFEM and the micromechanics averaging method (see Fig. 4). The four loading paths are subdivided into two subgroups: tensile loading and shear loading. The tensile case (see Fig. 4a) is implemented for both axial and transverse loading paths, depending on the pore orientation in the material. Similarly, the shear case (see Fig. 4b) contains both in-plane and out-of-plane loading paths, depending on the pore orientation. Since in the case of open pores the material has only five independent constants, only three of the loading paths are independent. However, the fourth-loading case is also presented for completeness.

Each loading case is analyzed at pore volume fraction c_p ranging from 0.2 to 0.6 for open pores and 0.1 to 0.5 for closed pores, respectively. Ranges of c_p are chosen based on the available experimentally observed values. The difference in the ranges of c_p for open and closed porosity is due to the pore size limitation in respective unit cells. For the case of closed pores, the minimum value of $c_p = 0.1$ is chosen so that the same number of data points are obtained for open and closed pore analyzes. The variations of effective elastic material properties with respect to c_p are obtained for both porous martensite and porous austenite. However, the results are only shown for porous austenite because the variations are similar for porous martensite. The effective pseudoelastic behavior is obtained by assuming the material to be initially stress-free and at the austenitic finish temperature ($A^{of} = 42°C$). Similarly, the shape memory effect behavior can be obtained by setting the temperature to be lower than $A^{os} = 22°C$. The material parameters chosen for the study are given in Table 2. The results obtained using the unit cell FEM and the micromechanics averaging method are presented in this section, while the comparison of the results and discussions are presented in Section 4.

3.1. Elastic behavior

Fig. 5 shows the variations of effective axial elastic modulus, E_A, effective transverse elastic modulus, E_T, effective plane strain bulk modulus, K_{PS}, effective out-of-plane shear modulus, G_A and effective in-plane shear modulus, G_T with respect to c_p. The variations in Fig. 5 represent differences in calculated material properties for periodic open and closed pore austenite using the UCFEM. As mentioned earlier, the variations for porous martensite are not shown here because they are similar to those of porous austenite. Only these five properties are calculated because as described in Section 2.1, hexagonal arrangement of both types of pores result in transverse material isotropy. The variations can be compared for open and closed porosity in the range of 0.2–0.4 c_p. As expected all material properties decrease with increasing c_p. It is

Table 2
Material parameters for dense NiTi SMA constitutive model[a]

Material parameters	Values
E^{A} (GPa)	70.0
E^{M} (GPa)	30.0
v	0.33
H	0.05
α^{A} (K^{-1})	22.0×10^{-6}
α^{M} (K^{-1})	10.0×10^{-6}
$\rho\Delta c$ (J/(m^{3}K))	0.0
$-\frac{\rho\Delta s_0}{H}$ (MPa/K)	7.0
M^{os} (°C)	18.0
M^{of} (°C)	−2.0
A^{os} (°C)	22.0
A^{of} (°C)	42.0
$\frac{\rho b^{A}}{H}$ (MPa)	140.0
$\frac{\rho b^{M}}{H}$ (MPa)	140.0

[a] See Lagoudas et al. (1996) and Qidwai and Lagoudas (2000a).

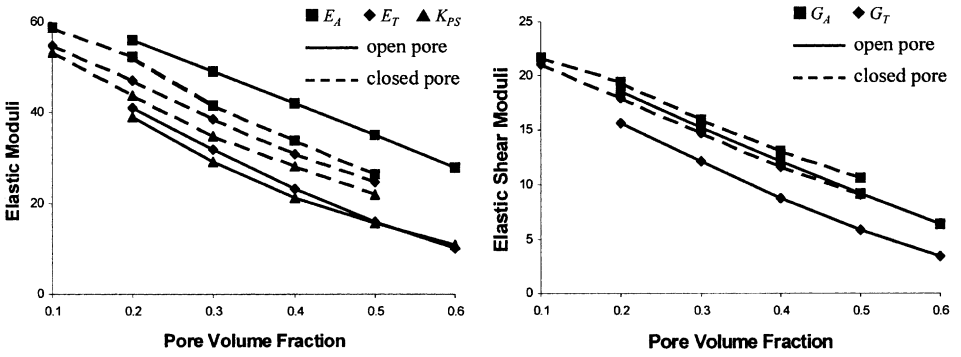

Fig. 5. Variation of effective axial elastic modulus, E_A, effective transverse elastic modulus, E_T, effective plane strain bulk modulus, K_{PS}, effective out-of-plane shear modulus, G_A and effective in-plane shear modulus, G_T with respect to pore volume fraction, as determined for open and closed pore periodic austenite using the UCFEM.

observed that E_A and G_A decrease linearly with c_p and the variation of G_A is similar for both open and closed pore material. The variations of E_A and E_T are similar for closed pore in the range of c_p considered. The differences in the variations of material properties such as E_A and E_T for closed pores is smaller than those for open pores. To explain this, note that in open pore unit cell lesser volume of material is projected in the transverse x-direction than in the axial z-direction (see Fig. 2). Also note that the amounts of material volume projected in the x- and z-directions for closed pore unit cell are closer in value than those between the open pore unit cell directions. That is, the closed pore material is more similar in the two directions (closer to isotropy) than the open pore material (closer to transverse isotropy), and this lesser differences in variations of material properties.

3.2. Transformation behavior

In this subsection, the results of porosity type and c_p on the effective phase transformation behavior of porous SMA are presented. In the UCFEM, except for the open pore axial loading case, the unit cell is

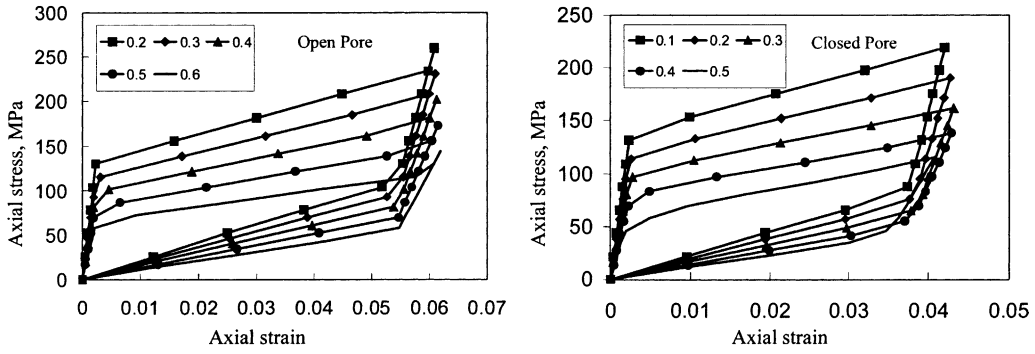

Fig. 6. Effective pseudoelastic stress–strain response of open and closed pore SMA for pore volume fractions ranging from 0.1 to 0.6 under axial loading calculated by using the UCFEM.

loaded from the stress-free state until an effective global strain of approximately 4% is obtained, and then unloaded fully. Stress concentration effects limit complete phase transformation throughout the matrix because of the resulting excessive stress levels locally in the material at some points, as will be discussed later in the text. The value of 4% is chosen to be consistent in comparison of results and also because it is sufficiently high to insure at least partial phase transformation within the unit cell. In the micromechanics averaging method, however, the material is loaded until complete phase transformation is obtained.

The effective axial pseudoelastic stress–strain response for the case of open and closed pores calculated by using the UCFEM is shown in Fig. 6. For this particular loading, the only non-zero effective stress component is the axial component, Σ_{zz}. The response is obtained for various c_p within the range of 0.1–0.6. Note in Fig. 6 that regardless of pore type the material initially behaves elastically and exhibits a distinct onset of the phase transformation in the matrix. By the end of the loading, complete phase transformation has taken place, and the dense SMA matrix is in the martensitic phase. Upon unloading, a distinct start of reverse phase transformation is observed. Full unloading results in the material returning to the austenitic phase and all the strain is recovered. With increasing pore volume fraction, the values of the applied stress required to initiate phase transformation in both forward and reverse phase transformation decreases. Also, reduction of the elastic stiffness of the material with increasing pore volume fraction is observed. The comparison of stress values and the elastic stiffness as described by the UCFEM and the micromechanics averaging method will be discussed in detail in Section 4.

The effective response under transverse loading for the case of open and closed porosity for various c_p calculated by the UCFEM is shown in Fig. 7. Note that only in the periodic open pore case is the initiation

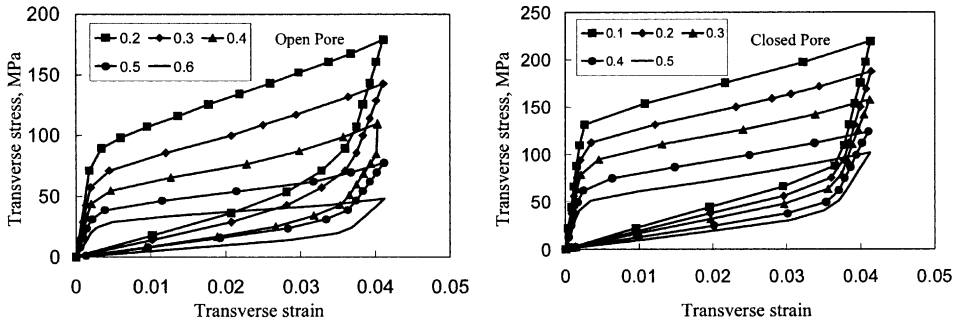

Fig. 7. Effective pseudoelastic stress–strain response of open and closed pore SMA for various pore volume fractions ranging from 0.1 to 0.6 under transverse loading calculated by using the UCFEM.

of phase transformation not distinctly obvious on the effective stress–strain curves. Additionally, the transition from elastic regime to phase transformation is sharper in the periodic closed pore case. All cases display decrease of the value of the applied stress necessary for the onset of transformation and reduction of the elastic stiffness of the material with increase in c_p.

In a similar fashion, effective response under in-plane and out-of-plane shear loading calculated by the UCFEM for various c_p exhibit similar trends of decreasing the value of the applied stress necessary for the onset of transformation and reduction of the elastic stiffness with increasing c_p as shown in Figs. 8 and 9, respectively.

The effective axial pseudoelastic stress–strain response for the case of open and closed pores calculated by the micromechanics averaging method is shown in Fig. 10. The other loading cases show similar trends as in the case of the UCFEM and are not presented here.

4. Discussion

This section is devoted to the comparison of the results obtained by the UCFEM and the MTM. First, the comparison of effective elastic material properties obtained by using the UCFEM and the micromechanics averaging method are shown in Fig. 11, where variations of effective axial elastic modulus, E_A, and effective transverse elastic modulus, E_T, of porous austenite are plotted with respect to c_p for open and

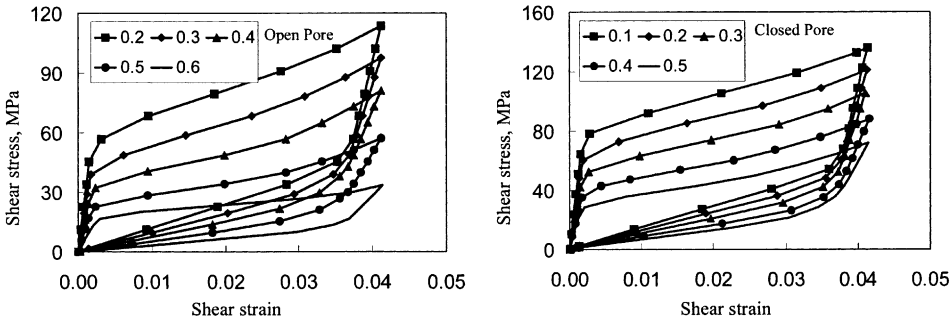

Fig. 8. Effective pseudoelastic stress–strain response of open and closed pore SMA for various pore volume fractions ranging from 0.1 to 0.6 under in-plane shear loading calculated by using the UCFEM.

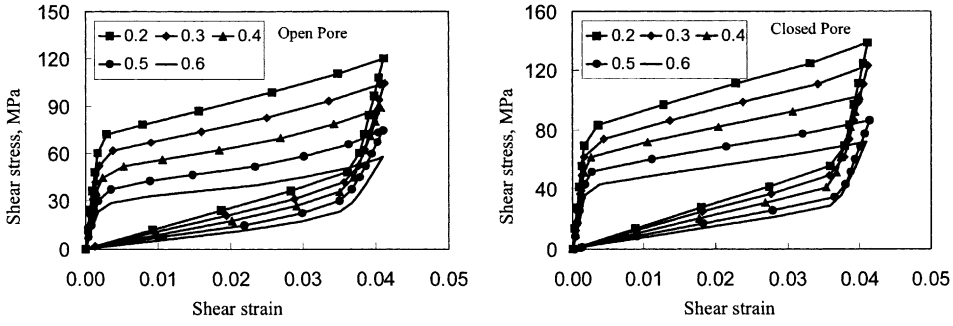

Fig. 9. Effective pseudoelastic stress–strain response of open and closed pore SMA for various pore volume fractions ranging from 0.1 to 0.6 under out-of-plane shear loading calculated by using the UCFEM.

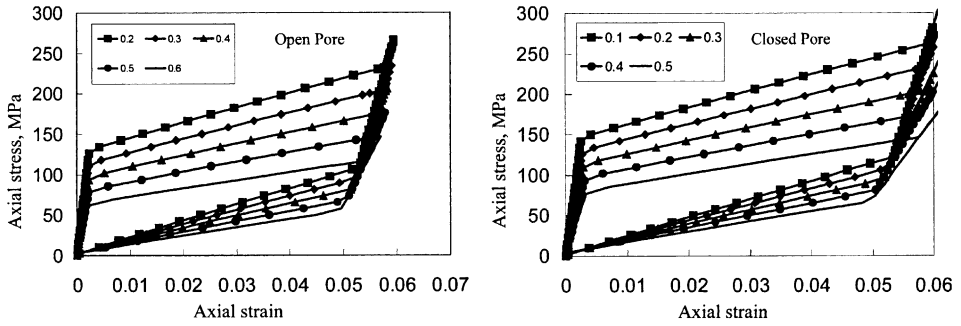

Fig. 10. Effective pseudoelastic stress–strain response of open and closed pore SMA for various pore volume fractions ranging from 0.1 to 0.6 under axial loading calculated by using the micromechanics averaging method (MTM).

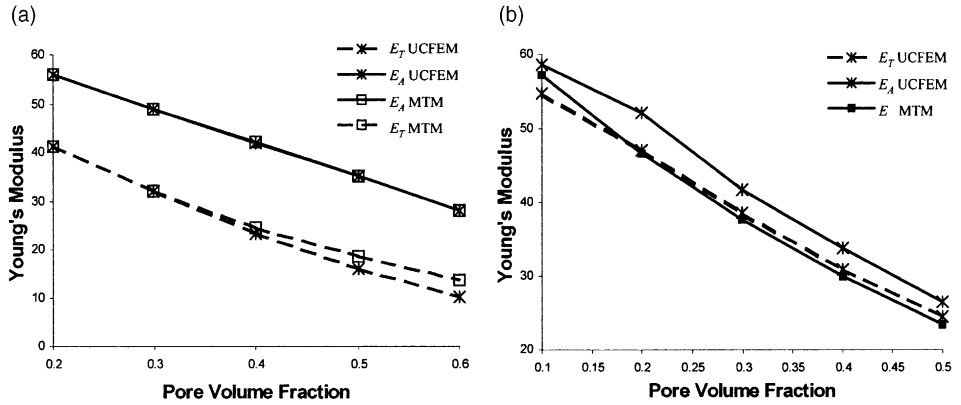

Fig. 11. Variation of effective axial modulus, E_A and effective transverse modulus, E_T, with respect to pore volume fraction as determined for (a) open and (b) closed pore austenite using the UCFEM and the micromechanics averaging method. The same variation is obtained for porous martensite.

closed pores. It is important to note that implementation of the micromechanics averaging method implicitly assumes a random distribution of open (cylindrical) pores in the x–y plane and a random distribution of closed (spherical) pores throughout the volume, respectively. These assumptions result in transverse isotropic symmetry for open pore SMA and isotropic material symmetry for closed pore SMA. This means that $E_A = E_T$ for closed pore micromechanics averaging method. Keeping this in mind, note that a good correlation is observed for normalized E_T for both open and pore cases through the two methods. Similarly, both methods calculate similar variation for E_A in the open pore case. However, there is a small difference in the variation of E_A for the closed pore case, which is attributed to difference in material symmetries. The same results are obtained for porous martensite but are not shown here.

The effective transformation behavior under axial loading is compared next for c_p of 0.2 and 0.5 for both open and closed pore (see Fig. 12). This provides a comparison for relatively low and high c_p. The open pore UCFEM, open pore MTM and closed pore MTM coincide for both volume fractions although the elastic unloading slope is slightly different in closed pore responses for both methods. This can be clearly seen in Fig. 11 where axial modulus is plotted with respect to the c_p. The main difference in results between the two methods is that closed pore UCFEM calculations show values of the applied stress for onset of the phase transformation significantly lower than in the other cases. This effect can be seen for all loading cases in Fig. 13 and both methods for open and closed pore SMA.

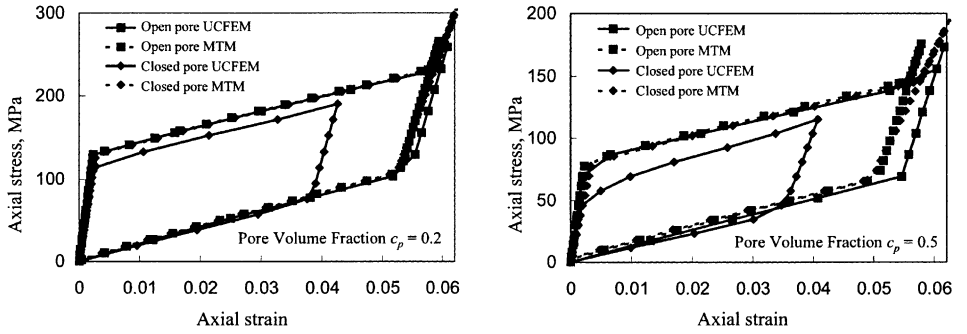

Fig. 12. Comparison of effective pseudoelastic stress–strain response of open and closed pore SMA for pore volume fraction of 0.2 and 0.5 under axial loading calculated by using the UCFEM and the micromechanics averaging method.

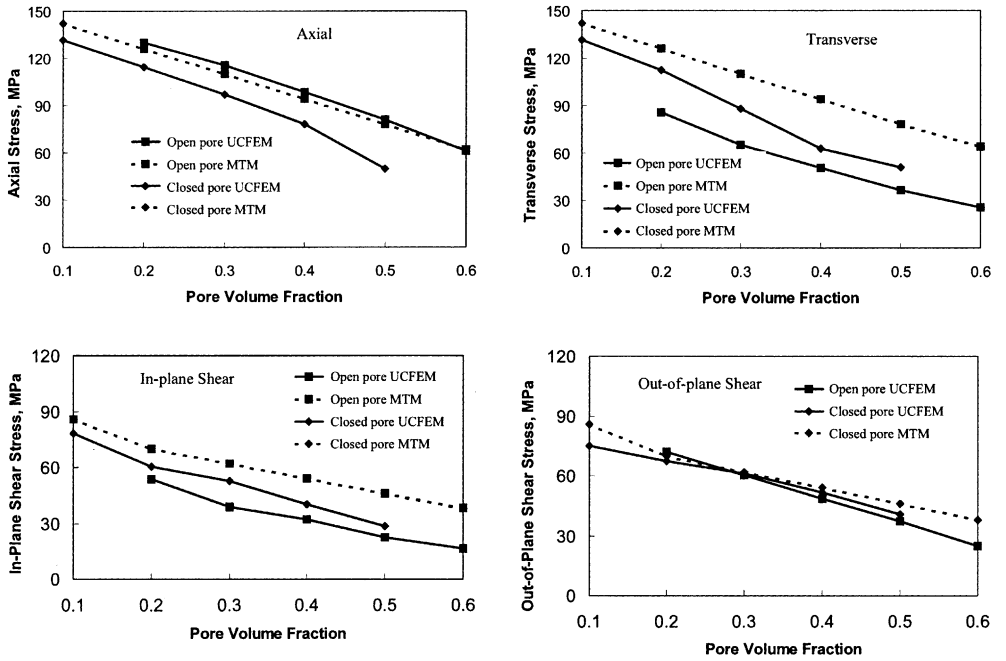

Fig. 13. Comparison of applied stress necessary to induce forward (A → M) phase transformation with respect to pore volume fraction for open and closed pore SMA calculated by using the UCFEM and the micromechanics averaging method under axial, transverse, in-plane shear and out-of-plane shear loading.

Understanding the source and nature of stress concentrations in the different types of porosity and methods of modeling them is crucial in understanding the calculated responses. In open (cylindrical) pore periodic distribution and the pore geometry does not lead to stress concentration. When the applied load is perpendicular to open cell porosity there is a stress concentration effect. On the other hand, in the case of closed (spherical) pores there is a geometric concentration factor regardless of the loading direction resulting in limited local transformation at a lower applied load. This effect is magnified near the pore and is dependent on the direction of applied load. The von Mises effective stress can be three to four times as high as the applied stress during phase transformation for closed (spherical) pores, and four to five times for

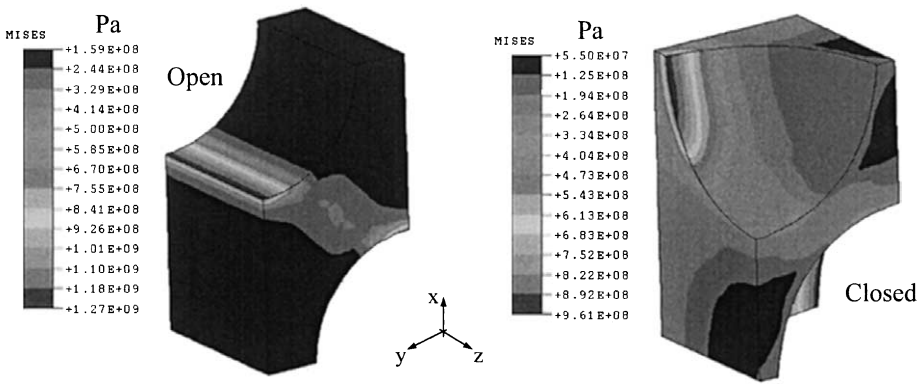

Fig. 14. von Mises effective stress contour plot of open and closed pore SMA for pore volume fraction of 0.4 at the end of transverse loading calculated by using the UCFEM.

open (cylindrical) pores when the loading is perpendicular to the axes of the cylinders. In both cases, the result is an inhomogeneous stress field in the matrix material (dense SMA) increasing non-proportionally during loading, which in turn induces inhomogeneous phase transformation throughout the matrix. In fact, as shown for c_p of 0.4 in Fig. 14 for both open and closed pores UCFEM at the end of transverse loading, many regions of the matrix remain elastic even when von Mises stress reaches values in GPa at certain material points locally.

The degree and scope of local inhomogeneity of transformation decide the value of applied stress necessary for the onset of transformation and level of distinction of phase transformation from elastic regime in the effective unit cell response. That is the reason that the value of applied stress necessary to induce phase transformation for closed pore UCFEM is consistently lower than that calculated from open pore UCFEM analyses. This is also the very reason that a lower maximum value of applied stress is imposed in the UCFEM to avoid large local stresses as evident from Fig. 14. Similarly, there is no distinct initiation of phase transformation on the effective stress–strain curve as seen in the case of transverse, in-plane shear and out-of-plane shear open and closed pore UCFEM responses in Figs. 7–9, respectively. Finally, it can be said that depending upon the c_p, shape of pore and direction of loading, transformation may take place locally at a much lower value of applied stress than the local stress in periodic unit cells.

The comparison between the transverse loading results highlights variations in calculated results due to basic assumptions associated with the UCFEM and the micromechanics averaging method. Fig. 15 contains the comparison for c_p of 0.2 and 0.5 for both open and closed pores. The periodic open pore applied stress necessary to induce phase transformation is less than the periodic closed pore applied stress as shown in Fig. 13. Whereas, the stress values for micromechanics averaging method are similar and larger than those of UCFEM. The micromechanics averaging method results also indicate that complete phase transformation has been achieved for both pore cases. Not shown here is the fact that the value of applied stress required in the UCFEM to achieve same levels of effective strain will cause local values of stress that are much greater than allowable stress due to concentrations as previously discussed. However, the micromechanics averaging method uses only the average value of stress, which is much lower than the actual stress due to concentration effects. Thus, the onset of the phase transformation occurs much later for the micromechanics averaging method than for the UCFEM. Another observation is that while the transformation does not take place throughout the matrix in the case of UCFEM, this is not the case if the micromechanics averaging method is used since all material points in the RVE are assumed to behave in the same fashion. Therefore, transformation occurs uniformly throughout the matrix, and complete trans-

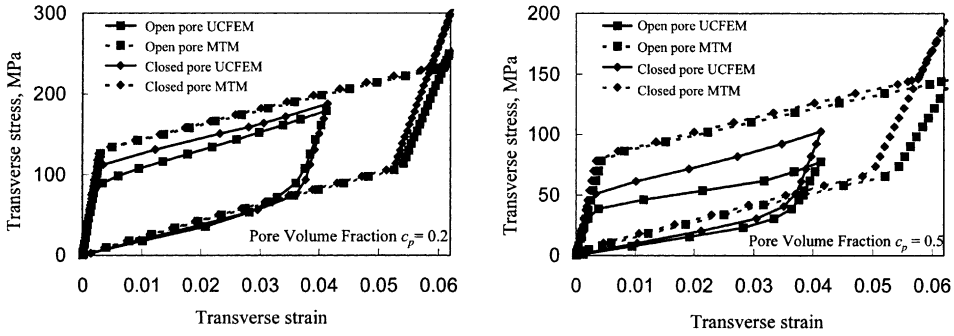

Fig. 15. Comparison of effective pseudoelastic stress–strain response of open and closed pore SMA for pore volume fraction of 0.2 and 0.5 under transverse loading calculated by using the UCFEM and the micromechanics averaging method.

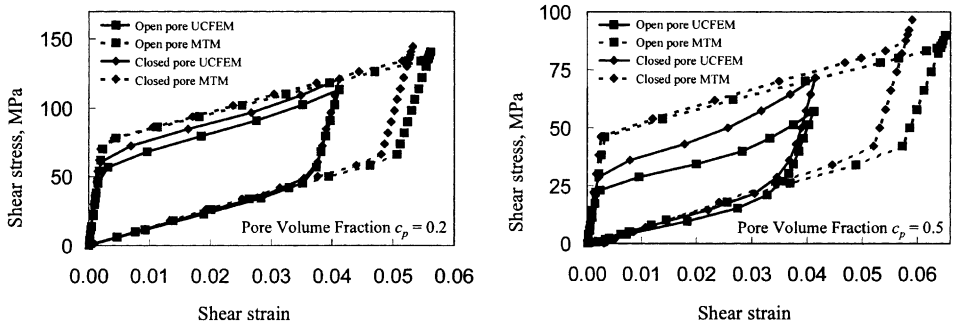

Fig. 16. Comparison of effective pseudoelastic stress–strain response of open and closed pore SMA for pore volume fraction of 0.2 and 0.5 under in-plane shear loading calculated by using the UCFEM and the micromechanics averaging method.

formation is obtained at a reasonable value of applied stress in the micromechanics averaging method. (The same value of applied stress would theoretically produce large plastic deformations at material points near the pore boundary in the periodic unit cell.)

Modeling method results in greater differences in the effective in-plane shear behavior than in the critical stress and transformation values only, as shown in Fig. 16. Note that at the higher c_p of 0.5, the rate of effective hardening is non-linear for UCFEM regardless of pore type. The results for the out-of-plane shear loading have better correlation in terms of critical applied stress and rate of hardening (see Fig. 17). The critical applied stresses for both in-plane shear and out-of-plane shear are shown in Fig. 13. The greatest difference in calculated results of the two methods is observed in the in-plane and transverse directions. This is a direct result of stress concentration, which is more severe in the two directions. It should also be noted that the difference between the two methods is always less for the closed pore case compared to the open pore case. This is due to the fact that even though stress concentration exists near the pore boundaries in closed pore case, it is less severe for the spherical pores than for the cylindrical pores especially under transverse or in-plane pure shear loading.

5. Conclusions

An in-depth thermomechanical analysis of porous SMA material has been carried out using micromechanical methods. Two methods, the UCFEM to analyze periodic distribution of pores and the

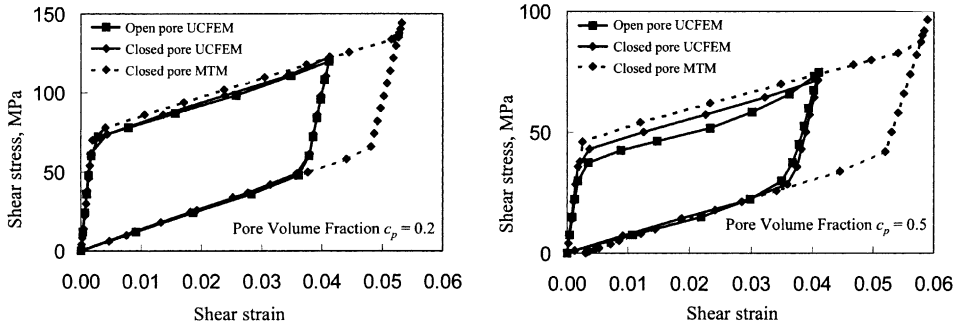

Fig. 17. Comparison of effective pseudoelastic stress–strain response of open and closed pore SMA for pore volume fraction of 0.2 and 0.5 under out-of-plane shear loading calculated by using the UCFEM and the micromechanics averaging method.

Mori–Tanaka averaging method (MTM) to analyze the random distribution of pores are employed. Two types of pores are assumed to exist in the dense SMA matrix: open (cylindrical) pores and closed (spherical) pores. The effective elastic and pseudoelastic isothermal responses have been calculated for different loading paths, including material hysteresis. Overall a good correlation between the two methods has been observed. The results obtained through the UCFEM are influenced by local stress concentrations, dependent on the pore volume fraction (c_p), pore shape and the direction of loading.

The comparison of the calculated results with experimental data has been omitted in this work and will be presented in future publication. One of the difficulties to overcome in the experiments is the fabrication of porous material with known SMA matrix properties.

The level of applied stress to initiate phase transformation calculated by the UCFEM is shown to be consistently lower than that calculated by the micromechanics averaging method for each loading case. This is a result of basic modeling assumption of average stresses in the micromechanics averaging method at each material point, which are significantly lower than the local stresses due to stress concentration in the UCFEM. Use of local values of stress at each material point also results in gradual transition between the elastic and transformation regimes in the effective stress–strain responses calculated by the UCFEM unlike those, which are calculated by the micromechanics averaging method and show distinct initiation of phase transformation. Another effect of the stress concentration near the pore boundaries is the smaller percentage of transformed matrix in the UCFEM compared to the micromechanics averaging method. In fact, large matrix volume remains in the elastic regime. This means that the observed effective transformation strain in the UCFEM is controlled by the local values of transformation strain in a small region around the pore.

Acknowledgements

The authors acknowledge the financial support of the Office of Naval Research grant no. M00014-99-1-1069 monitored by Dr. Roshdy Barsoum and the support from the Texas Higher Education Coordinating Board TD&T grant no. 000512-0278-1999. The computations performed by M.A. Qidwai and V.G. DeGiorgi were supported in part by a grant of HPC time from the DoD HPC Center at the Naval Research Laboratory, Washington, DC.

Appendix A. SMA constitutive model

The SMA constitutive model (Lagoudas et al., 1996; Qidwai and Lagoudas, 2000a) for isothermal conditions is briefly summarized below. The strain is given by

$$\varepsilon_{ij}^{m} = S_{ijkl}\sigma_{kl}^{m} + \varepsilon_{ij}^{tm}, \tag{A.1}$$

where ε_{ij}^{m} and σ_{ij}^{m} are the strain and stress in the SMA matrix and ε_{ij}^{tm} is the transformation strain. S_{ijkl} is the compliance tensor and is defined by the rule of mixtures as

$$S_{ijkl} = S_{ijkl}^{\mathrm{A}} + \xi(S_{ijkl}^{\mathrm{M}} - S_{ijkl}^{\mathrm{A}}). \tag{A.2}$$

In the equation above ξ is the volume fraction of the martensite phase and S_{ijkl}^{A} and S_{ijkl}^{M} are the compliance tensors of the austenite and martensite phases, respectively. The relation between the transformation strain tensor ε_{ij}^{tm} and the martensitic volume fraction ξ is expressed by

$$\dot{\varepsilon}_{ij}^{tm} = \Lambda_{ij}\dot{\xi}, \tag{A.3}$$

where Λ_{ij} is the transformation tensor which determines the transformation strain direction. Λ_{ij} is assumed to have the following form:

$$\Lambda_{ij} = \begin{cases} \frac{3}{2}H\frac{\sigma_{ij}^{m\prime}}{\bar{\sigma}^{m}}, & \dot{\xi} > 0 \\ H\frac{\varepsilon_{ij}^{t-r}}{\bar{\varepsilon}^{t-r}}, & \dot{\xi} < 0 \end{cases} \tag{A.4}$$

where H is the maximum uniaxial transformation strain, ε_{ij}^{t-r} is the transformation strain at the reversal of the transformation and

$$\bar{\sigma}^{m} = \sqrt{\frac{3}{2}}\|\sigma_{ij}^{m\prime}\|, \quad \sigma_{ij}^{m\prime} = \sigma_{ij}^{m} - \frac{1}{3}\sigma_{kk}^{m}\delta_{ij}, \quad \bar{\varepsilon}^{t-r} = \sqrt{\frac{2}{3}}\|\varepsilon_{ij}^{t-r}\|. \tag{A.5}$$

The thermodynamic force conjugate to ξ is given by

$$\pi = \sigma_{ij}^{m}\Lambda_{ij} + \tfrac{1}{2}\sigma_{ij}^{m}\Delta S_{ijkl}\sigma_{kl}^{m} + \rho\Delta s_0 T - \frac{\partial f}{\partial \xi} - \rho\Delta u_0 \tag{A.6}$$

where $f(\xi)$ is the hardening function, the terms with the prefix Δ indicate the difference of a quantity between the martensitic and austenitic phases and are given by

$$\Delta S_{ijkl} = S_{ijkl}^{\mathrm{M}} - S_{ijkl}^{\mathrm{A}}, \quad \Delta s_0 = s_0^{\mathrm{M}} - s_0^{\mathrm{A}}, \quad \Delta u_0 = u_0^{\mathrm{M}} - u_0^{\mathrm{A}}, \tag{A.7}$$

where s_0 and u_0 are specific entropy and internal energy at the reference state.

The transformation function Φ is defined in terms of the thermodynamic force π as

$$\Phi = \begin{cases} \pi - Y^{*}, & \dot{\xi} > 0 \\ -\pi - Y^{*}, & \dot{\xi} < 0 \end{cases} \tag{A.8}$$

where Y^{*} is the measure of internal dissipation due to the phase transformation. Constraints on the evolution of the martensitic volume fraction are expressed in terms the Kuhn–Tucker conditions as

$$\begin{aligned} &\dot{\xi} \geqslant 0, \quad \Phi(\sigma_{ij}^{m}, T, \xi) \leqslant 0, \quad \Phi\dot{\xi} = 0, \\ &\dot{\xi} \leqslant 0, \quad \Phi(\sigma_{ij}^{m}, T, \xi) \leqslant 0, \quad \Phi\dot{\xi} = 0. \end{aligned} \tag{A.9}$$

Finally, the hardening function $f(\xi)$ is given by

$$f(\xi) = \begin{cases} \frac{1}{2}\rho b^{\mathrm{M}}\xi^2 + (\mu_1 + \mu_2)\xi, & \dot{\xi} > 0 \\ \frac{1}{2}\rho b^{\mathrm{A}}\xi^2 + (\mu_1 - \mu_2)\xi, & \dot{\xi} < 0 \end{cases} \tag{A.10}$$

where ρb^{M}, ρb^{A}, μ_1 and μ_2 are transformation strain hardening constants. The material parameters for the above described model are summarized in Table 2.

References

ABAQUS, 1997. Standard User's Manual. Hibbit, Karlsson & Sorensen Inc.

Achenbach, J.D., Zhu, H., 1990. Effect of interphases on micro and macromechanical behavior of hexagonal-array fiber composites. Trans. ASME 57, 956–963.

Ayers, R.A., Simske, S.J., Bateman, T.A., Petkus, A., Sachdeva, R.L.C., Gyunter, V.E., 1999. Effects of nitinol implant porosity on cranial bone ingrowth and apposition after 6 weeks. J. Biomed. Mater. Res. 45 (1), 42–47.

Benveniste, Y., 1987. A new approach to the application of Mori–Tanaka's theory in composite material. Mech. Mater. 6, 147–157.

Birman, V., 1997. Review of mechanics of shape memory alloy structures. Appl. Mech. Rev. 50 (11), 629–645.

Boyd, J.G., Lagoudas, D.C., 1996. A thermodynamic constitutive model for the shape memory materials. Part I. The monolithic shape memory alloys. Int. J. Plast. 12 (6), 805–842.

Brinson, L.C., Lammering, R., 1993. Finite element analysis of the behavior of shape memory alloys and their applications. Int. J. Solids Struct. 30, 3261–3280.

Budiansky, B., 1965. On the elastic moduli of some heterogeneous materials. J. Mech. Phys. Solids 13, 223–227.

Buehler, W.J., Wiley, R.C., 1965. Nickel-base alloys. US Patent 3,174,851.

Buehler, W.J., Gilfrich, J.V., Wiley, R.C., 1963. Effects of low-temperature phase changes on the mechanical properties of alloys near composition TiNi. J. Appl. Phys. 34, 1475.

Cherkaoui, M., Sun, Q.P., Song, G.Q., 2000. Micromechanics modeling of composite with ductile matrix and shape memory alloy reinforcement. Int. J. Solids Struct. 37, 1577–1594.

Gavazzi, A.C., Lagoudas, D.C., 1990. On the numerical evaluation of Eshelby's tensor and its application to elastoplastic fibrous composites. Comput. Mech. 7, 13–19.

Gibson, L., Ashby, M., 1997. Cellular Solids, second ed. Cambridge Solid State Science Series, Cambridge University Press.

Govindjee, S., Hall, G.J., 1999. Computational aspects of solid–solid phase transformation modeling with a Gibbs function. Mathematics and Controls in Smart Structures. SPIE, International Society for Optical Engineering, Bellingham, WA, vol. 3667, pp. 302–313.

Graesser, E.J., Cozzarelli, F.A., 1994. A proposed three-dimensional constitutive model for shape memory alloys. J. Intell. Mater. Syst. Struct. 5, 78–89.

Green, R.J., 1972. A plasticity theory for porous solids. Int. J. Mech. Sci. 14, 215–224.

Gurson, A.L., 1977. Continuum theory of dictile rupture by void nucleation and growth: Part I – Yield criteria and flow rules for porous ductile media. J. Engng. Mater. Technol. 99, 2–15.

Hershey, A.V., 1954. The elasticity of an isotropic aggregate of anisotropic cubic crystals. J. Appl. Mech. 21, 236–240.

Hill, R., 1965. A self-consistent mechanics of composite materials. J. Mech. Phys. Solids 13, 213–222.

Hutchinson, J.W., 1970. Elastic–plastic behaviour of polycrystalline metals and composites. Proc. Roy. Soc. Lond. A 319, 247–272.

Itin, V.I., Gyunter, V.E., Shabalovskaya, S.A., Sachdeva, R.L.C., 1994. Mechanical properties and shape memory of porous nitinol. Mater. Charact. 32, 179–187.

Jeong, H.-Y., Pan, J., 1995. A macroscopic constitutive law for porous solids with pressure-sensitive matrices and its implications to plastic flow localization. Int. J. Solids Struct. 32 (24), 3669–3691.

Kröner, E., 1958. Berechnung der elastischen konstanten des vielkristalls aus den konstanten des einkristalls. Z. Phys. 151, 504–518.

Lagoudas, D.C., Bo, Z., Qidwai, M.A., 1996. A unified thermodynamic constitutive model for SMA and finite element analysis of active metal matrix composite. Mech. Compos. Mater. Struct. 3, 153–179.

Lagoudas, D.C., Boyd, J.G., Bo, Z., 1994. Micromechanics of active composites with SMA fibers. ASME J. Mater. Sci. Technol. 5, 337–347.

Lagoudas, D.C., Entchev, P.B., Qidwai, M.A., DeGiorgi, V.G., 2000a. Micromechanics of porous shape memory alloys. In: Redmont, J., Main, J. (Eds.), Proceedings of 2000 ASME International Mechanical Engineering Congress & Exposition, The American Society of Mechanical Engineers, New York, pp. 41–50.

Lagoudas, D.C., Entchev, P.B., Vandygriff, E.L., Qidwai, M.A., DeGiorgi, V.G., 2000b. Modeling of thermomechanical response of porous shape memory alloys. In: Lynch, C.S. (Ed.), Proceedings of SPIE, Smart Structures and Materials 2000. Active Materials: Behavior and Mechanics, vol. 3992. SPIE, pp. 496–508.

Lagoudas, D.C., Gavazzi, A.C., Nigam, H., 1991. Elastoplastic behavior of metal matrix composites based on incremental plasticity and the Mori–Tanaka averaging scheme. Comput. Mech. 8, 193–203.

Levitas, V.I., 1998. Thermomechanical theory of martensitic phase transformations in inelastic materials. Int. J. Solids Struct. 35, 889–940.

Li, B.-Y., Rong, L.-J., Li, Y.-Y., 1998a. Porous NiTi alloy prepared from elemental powder sintering. J. Mater. Res. 13, 2847–2851.

Li, B.-Y., Rong, L.-J., Li, Y.-Y., 1999. Microstructure and superelasticity of porous NiTi alloy. Sci. China E-42, 94.

Li, B.-Y., Rong, L.-J., Luo, X.-H., Li, Y.-Y., 1998b. Transformation behavior of sintered porous NiTi alloys. Metall. Mater. Trans. A 30A, 2753–2756.

Liang, C., Rogers, C.A., 1990. One-dimensional thermomechanical constitutive relations for shape memory materials. J. Intell. Mater. Syst. Struct. 1, 207–234.

Liang, C., Rogers, C.A., 1992. The multi-dimensional constitutive relations of shape memory alloys. J. Engng. Math. 26, 429–443.

Mori, T., Tanaka, K., 1973. Average stress in matrix and average energy of materials with misfitting inclusions. Acta Metall. 21, 119–146.

Nemat-Nasser, S., Hori, M., 1993. Micromechanics: overall properties of heterogeneous materials. North-Holland Series in Applied Mathematics and Mechanics, vol. 37. North-Holland.

Qidwai, M.A., Lagoudas, D.C., 2000a. Numerical implementation of a shape memory alloy thermomechanical constitutive model using return mapping algorithms. Int. J. Numer. Meth. Engng. 47, 1123–1168.

Qidwai, M.A., Lagoudas, D.C., 2000b. On thermomechanics and transformation surfaces of polycrystalline NiTi shape memory alloy material. Int. J. Plast. 16, 1309–1343.

Shabalovskaya, S.A., Itin, V.I., Gyunter, V.E., 1994. Porous Ni–Ti – a new material for implants and prostheses. Proceedings of the First International Conference on Shape Memory and Superelastic Technologies. SMST International Committee, MIAS, Monterey, CA, pp. 7–12.

Shevchenko, O.M., Gavrilyuk, G.V., Kokorin, V.V., Chernenko, V.A., 1997. Obtaining Fe–Ni–Co–Ti alloys having a thermoelastic martensite transformation. Powder Metall. Metal Ceramics 36 (1–2), 71–76.

Simske, S.J., Ayers, R.A., Bateman, T.A., 1996. Porous materials and tissue engineering. In: Ishawa, D. (Ed.), Porous Materials for Bone Engineering.

Tanaka, K., 1986. A thermomechanical sketch of shape memory effect: One-dimensional tensile behavior. Res Mech. 18, 251–263.

Thangaraj, K., Chen, Y.-C., Salama, K., 2000. Fabrication of porous NiTi shape memory alloy by elemental powder sintering. In: Redmont, J., Main, J. (Eds.), Proceedings of 2000 ASME International Mechanical Engineering Congress & Exposition, The American Society of Mechanical Engineers, New York, pp. 59–63.

Vandygriff, E.C., Lagoudas, D.C., Thangaraj, K., Chen, Y.-C., 2000. Porous shape memory alloys, Part I: Fabrication and characterization. Proceedings of ASC 15th Annual Technical Conference. Technomic Publishing Co., Inc., Lancaster, PA, pp. 239–247.

Wayman, C.M., 1983. Phase transformations, nondiffusive. In: Cahn, R.W., Haasen, P. (Eds.), Physical Metallurgy, North-Holland Physics Publishing, New York, pp. 1031–1075.

Weng, G.J., 1984. Some elastic properties of reinforced solids, with special reference to isotropic ones, containing spherical inclusions. Int. J. Engng. Sci. 22, 845–856.